Journal of Elasticity (2026) 158:12
https://doi.org/10.1007/s10659-026-10187-3

RESEARCH

Shear Models in Finite Elasticity

Federico Oyedeji Falope[1] · **Luca Lanzoni**[1] · **Angelo Marcello Tarantino**[1]

Received: 15 November 2025 / Revised: 15 November 2025 / Accepted: 16 January 2026 /
Published online: 28 January 2026

Abstract
Having been studied for a long time, simple and pure shear deformation models are well known in elasticity. For small deformations, these two shear models differ only by a rigid rotation. On the contrary, for large deformations, the two models do not differ only by a rigid rotation. Therefore, in the latter situation, one cannot expect both models to fit the same constitutive properties for a prescribed form of the stored energy function. The kinematic and static differences between the two shear models, as well as their inadequacies for simulating experimental evidences, are discussed in this paper. To overcome these critical issues, a study was developed, which led quite naturally to the definition of a new shear deformation model, here called *purely angular shear*, based on the direct extension of the linearized pure shear model. The new model, characterized by a simple and immediate physical meaning, is particularly suitable for matching experimental tests.

Keywords Finite elasticity · Hyperelasticity · Shear deformation · Pure shear · Simple shear · Purely angular shear · Compressible materials

Mathematics Subject Classification 74B20 · 74G75 · 74K10

1 Introduction

The concept of shear stress is a classic topic of elasticity, which appears to have been introduced in 1713 by the French mathematician Parents [1, 2] and [3]. Later shear stress was extensively developed by Coulomb for applications like beam bending and soil mechanics [4]. His research on the shear strength of materials, originally for masonry and other brittle materials, led to a fundamental understanding of how materials fail under stress, particularly through sliding planes. Cauchy formalized the concept of shear stress as three components of the stress tensor in 1822, laying the foundation for modern continuum mechanics [5–7]

✉ L. Lanzoni
luca.lanzoni@unimore.it

F.O. Falope
federicooyedeji.falope@unimore.it

A.M. Tarantino
angelomarcello.tarantino@unimore.it

[1] DIEF, Università di Modena e Reggio Emilia, via P. Vivarelli 10, 41125, Modena, Italy

and [8]. This made it possible to analyze the mechanical behavior of solids to understand how these deform under external actions that twist or slide them.

A general analysis for the finite shear deformations can be found in Boulanger and Hayes [9] and references therein. Under arbitrary deformation, in [9], two main problems are solved. The first is the determination of all pairs of material line elements which are unsheared. The second is the identification of the pairs of material line elements which exhibit the maximum shear (see also [10]). Subsequently, the same authors produced numerous contributions on the geometric aspects of shear deformations [11–17] and [18].

Response functions describing the constitutive behavior of materials subjected to shear stresses have also been extensively studied. The most popular models are the *simple shear* and the *pure shear*. Given his clear mechanical meaning in the linearized elasticity, Rivlin (1948) [19] was the first to propose the strain formulation of the simple shear in the framework of finite elasticity, considering a block of incompressible material. The simple shear has since received much attention in the literature, because it has played a role as a basic pilot problem capable of illustrating some key features for the nonlinear theory, as the presence of normal stresses in addition to shear stresses. Simple shear tests are not easy to perform and consequently few experimental works are available (see the paper of Mooney (1944) [20] and the more recent work of Brown (2006) [21]). This is because to maintain a simple shear plane deformation, the corresponding two in-plane shear stress components, but also all three normal stress components, must be applied to the sample. By inverting the problem formulation,[1] it has been demonstrated that the (plane) pure shear stress state produces a deformation field that does not coincide with the simple shear deformation, but with a simple shear deformation superimposed upon a triaxial stretch (see Moon and Truesdell [23], Horgan and Murphy [24], Mihai and Goriely [25], Destrade, Murphy and Saccomandi [26] and Thiel et al. [27]).

The pure shear model is technically accomplished by subjecting a sheet to axial extension and evaluating the shear deformation with a reference system inclined at an angle of $\pi/4$. The first pure shear experiments on thin sheets of rubber-like material were performed by Treloar (1944) [28]. Further experimental investigations have been carried out by Rivlin and Saunders [29] and more recently by Sasso et al. [30]. For this model it can be observed that the dimension orthogonal to the extension direction is preserved and this is not consistent with what can be expected from a shear deformation. Furthermore (as will be shown below), the pure shear model is not able to reproduce the linearized case.

In the case of small deformations, the simple shear can be considered as a pure shear followed by a rigid rotation. When the deformations become large, the two shear models not only do not differ by a rigid rotation, but they are really physically different. This is because their application provides different deformation and stress fields (as will be shown below).

There are few studies in the literature regarding the comparison of the two shear models under large deformations. For example, Segal [31], studying, from a continuum standpoint, the deformation modes on structural evolution under severe plastic deformation, concluded that all possible deformation states range from pure shear to simple shear. For the two shear models, Morreira and Nunes [32], considering samples composed of silane modified polymer, performed an extensive experimental campaign. Their results showed that the constitutive law, giving the principal Cauchy stress as a function of the relative principal stretch,[2]

[1] The stress formulation of the shear problem has been defined by Truesdell [22] as the "most illuminating homogeneous static deformation".

[2] The data obtained satisfy the Baker-Ericksen inequality, which establishes that the greater principal stress always occurs in the direction of the greater principal stretch [33].

presents a divergence between simple and pure shear, which increases considerably for large stretch values. Simple and pure shear deformation modes were studied by Pardis, Ebrahimi and Kim [34], using finite element method. Considering plane samples of pure aluminum deformed beyond the yield limit, they found that for these samples the deformation mode is neither simple nor pure shear. Therefore, to evaluate the effective shear deformation, they proposed to modify the simple shear model by means of additional increments of distortional shear deformation such as to change suitable the geometry of the deformed sample.

This paper is devoted to the measure of shear deformation in finite elasticity and is organized as follows. After some reminders in Sect. 2 of the shear deformation in the linearized theory, in Sect. 3 the simple and pure shear models are studied in detail, showing the kinematic and static differences. To avoid the difficulties encountered with these two models, the purely angular shear model is presented in Sect. 4. The displacement field and deformation tensors are determined. A Lagrangian analysis is then performed in order to formulate the boundary value problem for a material cube. The Piola-Kirchhoff and Cauchy stress fields were subsequently determined. Some applications are performed in Sect. 5. Section 6 closes the paper by summarizing the results obtained.

2 Notation and Shear in Linearized Elasticity

Let us consider a hyperelastic body $\bar{\mathcal{B}}$ composed of a homogeneous, isotropic and compressible material. Reference is made to a Cartesian coordinate system $\{O,\ X,\ Y,\ Z\}$ to identify the body with the closure of a regular domain of the three-dimensional Euclidean space $\mathcal{E}$.

The undeformed configuration $\bar{\mathcal{B}}$ of the body is assumed as the reference configuration, whereas the deformed configuration is given by the deformation $\mathbf{f}: \bar{\mathcal{B}} \to \mathcal{V}$.[3] As usual, deformation $\mathbf{f}$ is a smooth enough, injective and orientation-preserving vector field (in the sense that $\det(\mathrm{Grad}\,\mathbf{f}) > 0$). The deformation of a generic material point P can be expressed by the well-known relationship

$$\mathbf{f}(P) = \mathbf{s}(P) + \mathbf{id}(P), \tag{1}$$

where $\mathbf{id}(P)$ and

$$\mathbf{s}(P) = u(P)\mathbf{i} + v(P)\mathbf{j} + w(P)\mathbf{k} \tag{2}$$

are the position and displacement vectors of the point P. In expression (2), the functions $u(P)$, $v(P)$ and $w(P)$ denote the scalar components of $\mathbf{s}(P)$, whereas $\mathbf{i}$, $\mathbf{j}$ and $\mathbf{k}$ are the unit vectors. The application of the material gradient operator $\mathrm{Grad}(\cdot)$ to (1) gives

$$\mathbf{F} = \mathbf{H} + \mathbf{I}, \tag{3}$$

where $\mathbf{F}: \bar{\mathcal{B}} \to Lin^+$ and $\mathbf{H}: \bar{\mathcal{B}} \to Lin$ ([4]) are the deformation and displacement gradients, respectively. The symbol $\mathbf{I}$ denotes the identity tensor. We assign the shape of a cube to the body $\mathcal{B}$ ([5])

$$\mathcal{B} = \{(X,\ Y,\ Z) \mid 0 < X < a,\ 0 < Y < a,\ 0 < Z < a\},$$

where a is the length of the side.

[3] $\mathcal{V}$ is the vector space associated with $\mathcal{E}$.

[4] Lin is the set of all (second order) tensors, whereas Lin^+ is the subset of tensors with positive determinant.

[5] In reality, because homogeneous deformations will be considered, the shape of the body is irrelevant.

In the linearized elasticity, it is assumed that all nine (dimensionless) components of the tensor $\mathbf{H}$ are very small quantities: $\left|[\mathbf{H}]_{ij}\right| \ll 1$ (with $i, j = x, y$ and z). By applying the theorem of additive decomposition to the above linearized displacement gradient $\mathbf{H}$, the skew-symmetric tensor of infinitesimal rigid rotation $\mathbf{W}$ and the symmetric tensor of infinitesimal strain $\mathbf{E}$ are obtained ($\mathbf{H} = \mathbf{W} + \mathbf{E}$)

$$[\mathbf{W}] = \left[\frac{1}{2}\left(\mathbf{H} - \mathbf{H}^{\mathrm{T}}\right)\right] = \begin{bmatrix} 0 & -\omega_z & \omega_y \\ \omega_z & 0 & -\omega_x \\ -\omega_y & \omega_x & 0 \end{bmatrix}, \tag{4}$$

$$[\mathbf{E}] = \left[\frac{1}{2}\left(\mathbf{H} + \mathbf{H}^{\mathrm{T}}\right)\right] = \begin{bmatrix} \varepsilon_x & \frac{1}{2}\gamma_{xy} & \frac{1}{2}\gamma_{xz} \\ \frac{1}{2}\gamma_{xy} & \varepsilon_y & \frac{1}{2}\gamma_{yz} \\ \frac{1}{2}\gamma_{xz} & \frac{1}{2}\gamma_{yz} & \varepsilon_z \end{bmatrix}, \tag{5}$$

where

$$\omega_x = \frac{1}{2}\left(\frac{\partial w}{\partial y} - \frac{\partial v}{\partial z}\right), \quad \omega_y = \frac{1}{2}\left(\frac{\partial u}{\partial z} - \frac{\partial w}{\partial x}\right), \quad \omega_z = \frac{1}{2}\left(\frac{\partial v}{\partial x} - \frac{\partial u}{\partial y}\right), \tag{6}$$

$$\varepsilon_x = \frac{\partial u}{\partial x}, \quad \varepsilon_y = \frac{\partial v}{\partial y}, \quad \varepsilon_z = \frac{\partial w}{\partial z}, \tag{7}$$

$$\gamma_{xy} = \frac{\partial u}{\partial y} + \frac{\partial v}{\partial x}, \quad \gamma_{xz} = \frac{\partial u}{\partial z} + \frac{\partial w}{\partial x}, \quad \gamma_{yz} = \frac{\partial v}{\partial z} + \frac{\partial w}{\partial y}. \tag{8}$$

The components ω_i denote the infinitesimal rigid rotations, ε_i the infinitesimal normal strains and γ_{ij} the infinitesimal shear strains, respectively.

The deformation of the *simple shear* (applied to the XY plane) is[6]

$$\begin{cases} x = X + kY \\ y = Y \\ z = Z \end{cases}, \tag{9}$$

where k is a positive constant called the amount of shear.[7] These expressions indicate that the displacement component $u = x - X$ grows proportionally to the distance from the X axis, which is measured by the Y variable. The other two displacement components, v and w, are zero.

The displacement gradient computed for (9) has a single non-zero component: $\mathrm{H}_{xy} = k$, and the rotation and strain tensors take the following forms:

$$[\mathbf{W}] = \begin{bmatrix} 0 & \frac{1}{2}k & 0 \\ -\frac{1}{2}k & 0 & 0 \\ 0 & 0 & 0 \end{bmatrix}, \qquad [\mathbf{E}] = \begin{bmatrix} 0 & \frac{1}{2}k & 0 \\ \frac{1}{2}k & 0 & 0 \\ 0 & 0 & 0 \end{bmatrix}, \tag{10}$$

where, since k is an infinitesimal quantity, $\tan\gamma_{xy} \simeq \gamma_{xy} = k$ and $\omega_z = -\frac{1}{2}k$. Considering a cube with unit sides ($a = 1$), the geometric meaning of these two transformations is illustrated in Fig. 1. In this figure, the first image displays the infinitesimal rigid rotation of the

[6] The variables (X, Y, Z) indicate the coordinates of a generic material point P in the undeformed configuration, while the triple (x, y, z) corresponds to the position of the same point in the deformed configuration.

[7] Obviously, similar definitions apply to the XZ and YZ planes.

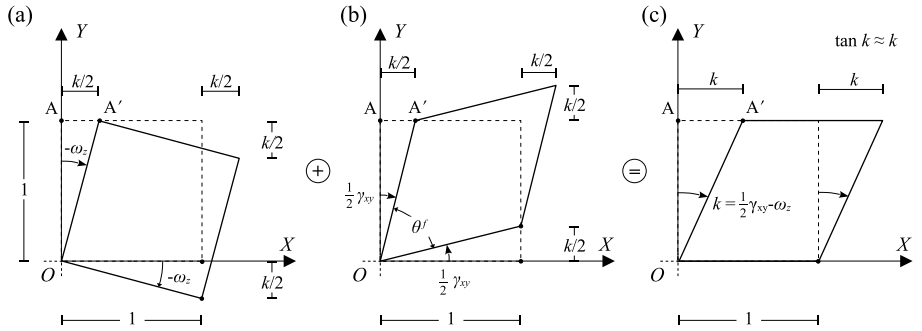

Fig. 1 Simple shear in the linearized elasticity theory. Composition of an infinitesimal rigid rotation (a) with a pure shear strain (b). Kinematics of simple shear(c)

unit plane element (understood as the base of the cube) and the second image shows the *pure shear strain*[8] of the same plane element. Summing, the deformed configuration generated by the simple shear is obtained (cf. Fig. 1c). It is important to note that this superposition holds if and only if the constant k is very small.

Note that, since all the angles involved in Fig. 1 are very small, point A moves to A', orthogonally to the Y axis. The shear strain γ_{xy} measures the variation of the initial right angle: $\gamma_{xy} = \frac{\pi}{2} - \theta^f$ (expressed in radians), where θ^f is the final angle formed by the two linear sides (initially parallel to the reference axes X and Y) after the deformation (cf. Fig. 1b). The shear strain γ_{xy} is positive when, due to deformation, the angle between the X and Y axes decreases.

The in-plane principal strains of the strain tensor $(10)_2$ are opposite, $\varepsilon_1 = -\varepsilon_2 = \frac{1}{2}k$, and the out-of-plane principal strain is zero, $\varepsilon_3 = 0$. Therefore, both pure and simple shear strains do not produce variations in area and volume[9]

$$da' - da = (\varepsilon_1 + \varepsilon_2)\, da = 0, \qquad dv' - dv = (\varepsilon_1 + \varepsilon_2 + \varepsilon_3)\, dv = 0. \tag{11}$$

By substituting the strain tensor $(10)_2$ into the linear Navier constitutive law: $\mathbf{T} = 2\mu\mathbf{E} + \lambda\vartheta\mathbf{I}$, where μ and λ are the Lamé constants and, for the case considered, $\vartheta = \mathrm{tr}\mathbf{E} = 0$ (i.e. absence of volume variation), the shear stress tensor is immediately evaluated

$$[\mathbf{T}] = \begin{bmatrix} 0 & \mu k & 0 \\ \mu k & 0 & 0 \\ 0 & 0 & 0 \end{bmatrix}. \tag{12}$$

This tensor, with only the T_{xy} and T_{yx} components non-zero, represents a *state of pure shear stress*. Therefore, a state of pure shear stress corresponds to a state of pure shear strain and vice versa. *In general, this property is not verified in finite elasticity.*

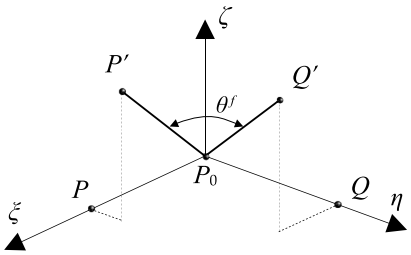

Fig. 2 Shear deformation component γ_{xy} in the local reference system $\{P_o, \xi, \eta, \zeta\}$

3 Simple Shear and Pure Shear Models in Finite Elasticity. Kinematic and Static Considerations

Always remaining in the context of homogeneous deformations, below the assumption of small deformations is removed and the definition of the large shear deformation component γ_{xy} is recalled. To evaluate γ_{xy} in finite elasticity, consider two elementary fibers oriented along the X and Y axes as shown in Fig. 2 (see, e.g., [9])

$$(P - P_0) = dX\,\mathbf{i}, \quad (Q - P_0) = dY\,\mathbf{j}. \tag{13}$$

The deformed images of these two fibers, namely

$$(P' - P_0) = dX\,\mathbf{Fi}, \quad (Q' - P_0) = dY\,\mathbf{Fj}, \tag{14}$$

subtend the angle θ^f defined by

$$\cos\theta^f = \frac{(P' - P_0)\cdot(Q' - P_0)}{|(P' - P_0)|\,|(Q' - P_0)|}. \tag{15}$$

By introducing the (symmetric and positive definite) right Cauchy-Green tensor, $\mathbf{C} = \mathbf{F}^{\mathrm{T}}\mathbf{F}$, together with the Green-St. Venant tensor, $2\mathbf{E} = \mathbf{C} - \mathbf{I}$, which takes into account only the pure deformation, and noting that $\cos\theta^f = \cos\left(\frac{\pi}{2} - \gamma_{xy}\right) = \sin\gamma_{xy}$, the previous expression (15) can be rewritten as

$$\sin\gamma_{xy} = \frac{2\mathrm{E}_{xy}}{\sqrt{1 + 2\mathrm{E}_{xx}}\sqrt{1 + 2\mathrm{E}_{yy}}}. \tag{16}$$

It is useful to rewrite the Green-St. Venant tensor in terms of the displacement gradient $\mathbf{H}$, namely

$$\mathbf{E} = \frac{1}{2}\left(\mathbf{H} + \mathbf{H}^{\mathrm{T}} + \mathbf{H}^{\mathrm{T}}\mathbf{H}\right). \tag{17}$$

It is then evident that the tensor $\mathbf{E}$ is composed of a linear part, $\frac{1}{2}\left(\mathbf{H} + \mathbf{H}^{\mathrm{T}}\right)$, formally similar to the strain tensor of linearized theory (5) and a quadratic part, $\frac{1}{2}\mathbf{H}^{\mathrm{T}}\mathbf{H}$, which characterizes the nonlinear kinematic effects.[10] Since the linearization of the Green-St. Venant tensor

[8] Historically, the term pure has been used as a synonym for irrotational.

[9] The apex $(\cdot)'$ denotes the corresponding quantity in the deformed configuration.

[10] Note how in the exact theory of deformation, the Green-St. Venant tensor $\mathbf{E}$ has terms, in the components of $\mathbf{H}$, of degree no higher than the second.

provides the linear strain tensor, this tensor is suitable to describe the large/small transition that the shear deformation component γ_{xy} undergoes when passing from the nonlinear to linearized elasticity. For this reason, to denote the Green-St. Venant tensor we use the same symbol $\mathbf{E}$ as the strain tensor (5).

The constitutive properties of a hyperelastic material are described by the stored energy function ω. If the function ω is frame-indifferent, homogeneous and isotropic, then it depends only on the principal invariants I_i, with $i = 1$, 2 and 3, of the Cauchy-Green strain tensors. With these assumptions, the constitutive law ($\mathbf{T}_R = \partial\omega/\partial\mathbf{F}$) takes the following form:

$$\mathbf{T}_R = 2\left(\frac{\partial\omega}{\partial I_1} + I_1\frac{\partial\omega}{\partial I_2}\right)\mathbf{F} - 2\frac{\partial\omega}{\partial I_2}\mathbf{B}\mathbf{F} + 2I_3\frac{\partial\omega}{\partial I_3}\mathbf{F}^{-\mathrm{T}}, \tag{18}$$

where the tensor $\mathbf{T}_R$ denotes the (first) Piola-Kirchhoff stress tensor. In the above expression, $\mathbf{B} = \mathbf{F}\mathbf{F}^{\mathrm{T}}$ is the left Cauchy-Green strain tensor and $\mathbf{B}\mathbf{F} = \mathbf{F}\mathbf{C}$. Piola-Kirchhoff stresses are the Lagrangian stresses (to be understood as nominal), while the corresponding Eulerian stress measure is that of Cauchy, namely the corresponding stresses in the deformed configuration (to be understood as true). The Cauchy stress tensor $\mathbf{T}$ can be obtained from the Piola-Kirchhoff stress tensor $\mathbf{T}_R$ through the following well-known transformation:

$$\mathbf{T}_R = \mathbf{T}\mathbf{F}^{\star}, \tag{19}$$

where $\mathbf{F}^{\star} = (\det\mathbf{F})\mathbf{F}^{-\mathrm{T}}$ is the cofactor of the tensor $\mathbf{F}$.[11]

3.1 Simple Shear Model

Presumably, the deformation in the linearized elasticity known as simple shear and illustrated by Fig. 1c induced initially Rivlin [19] to adopt the displacement field form (9) to describe the simple shear also in finite elasticity. In this context, the simple shear has been discussed and analyzed since Truesdell and Noll [33], Green and Zerna [35], Ogden [36] and Gurtin, Fried and Anand [37]. However, this extension *tout court* to the nonlinear case has raised doubts and shown substantial differences with the linear case. For example, Rivlin [19] himself highlighted that, unlike the linear case, to maintain the simple shear deformation it is now necessary to apply (in-plane and out-of-plane) normal stresses in addition to the shear stresses.

With the parameter k assumed not to be small, from (9) the following deformation gradient is obtained:

$$[\mathbf{F}] = \begin{bmatrix} 1 & k & 0 \\ 0 & 1 & 0 \\ 0 & 0 & 1 \end{bmatrix}. \tag{20}$$

Through its definition, from the above tensor $\mathbf{F}$, the right Cauchy-Green tensor $\mathbf{C}$ can be determined. The eigenvalues of the tensor $\mathbf{C}$ are

$$\begin{cases} \lambda_1^2 = \frac{2+k^2}{2} + \frac{k}{2}\sqrt{4+k^2} \\ \lambda_2^2 = \frac{2+k^2}{2} - \frac{k}{2}\sqrt{4+k^2} \\ \lambda_3^2 = 1 \end{cases}, \tag{21}$$

[11] The tensor $\mathbf{F}$ is invertible by its definition.

which coincide with the squares of the principal stretches. From the first two expressions we get: $\lambda_1^2\lambda_2^2 = 1$, and furthermore: $\lambda_1\lambda_2 = 1$, being the stretches strictly positive. This last relation shows that in the simple shear the in-plane stretches are reciprocal, $\lambda_1 = 1/\lambda_2$. From these considerations about the stretches, it follows that, similarly to the linear case (cf. (11)), the simple shear in finite elasticity is an area and volume preserving deformation

$$da' = da\left|\mathbf{F}^{\star}\mathbf{k}\right| = da, \qquad dv' = dv\,(\det\mathbf{F}) = dv. \tag{22}$$

This is a strong limitation for the simple shear model because it can only be applied to the class of incompressible materials.

We continue to examine kinematic aspects by computing the Green-St. Venant tensor

$$[\mathbf{E}] = \frac{1}{2}\begin{bmatrix} 0 & k & 0 \\ k & k^2 & 0 \\ 0 & 0 & 0 \end{bmatrix}. \tag{23}$$

In linearized elasticity, the strain tensor $(10)_2$ contains only two shear strain components, $\mathrm{E}_{xy} = \mathrm{E}_{yx} = \frac{1}{2}k$, due exclusively to an angular deformation. In the Green-St. Venant tensor (23) the same components appear (now with large k), but in addition the quadratic component $\mathrm{E}_{yy} = \frac{1}{2}\left(\frac{\partial u}{\partial Y}\right)^2 = \frac{1}{2}k^2$ is present. This nonlinear term is due to an extensional deformation. In fact, the material fibers, originally oriented along the Y axis, are inclined and elongated. Thus, in finite elasticity, simple shear deformation produces combined angular and extensional deformation effects. Moreover, the term E_{yy} causes the loss of the pure shear strain condition defined in the linearized elasticity through form of the strain tensor $(10)_2$.

Using (23), formula (16) gives the sine of γ_{xy} for the simple shear model

$$\sin\gamma_{xy} = \frac{k}{\sqrt{1+k^2}}. \tag{24}$$

The simple shear kinematics can be linearized by assuming that the constant k is an infinitesimal quantity. Then, k^2 can be neglected, and (23) simplifies to $(10)_2$. Similarly, $(10)_1$ is retrieved by the decomposition $\mathbf{F} = \mathbf{I} + \mathbf{W} + \mathbf{E}$. Furthermore, (24) reduces to: $\sin\gamma_{xy} \simeq \gamma_{xy} = k$.

For incompressible materials, Piola-Kirchhoff stress tensor cannot be evaluated with formula (18), but the following constitutive equation must be used:

$$\mathbf{T}_R = -p\mathbf{F}^{-\mathrm{T}} + 2\left(\frac{\partial\tilde{\omega}}{\partial I_1} + I_1\frac{\partial\tilde{\omega}}{\partial I_2}\right)\mathbf{F} - 2\frac{\partial\tilde{\omega}}{\partial I_2}\mathbf{B}\mathbf{F}, \tag{25}$$

where the stored energy function $\tilde{\omega}$ depends only on the two principal invariants I_1 and I_2, and p denotes the reactive pressure needed to satisfy the kinematical constraint of incompressibility $\det\mathbf{F} = 1$. To apply (25) it is necessary to assign a specific shape to the function $\tilde{\omega}$, calculate the tensors $\mathbf{F}^{-\mathrm{T}}$ and $\mathbf{B}\mathbf{F}$ on the basis of the deformation gradient (20) and determine the invariants with the stretches (21): $I_1 = I_2 = 3 + k^2$. The constant p is computed by using boundary conditions.[12] Once the Piola-Kirchhoff stress tensor has been obtained, the

[12] Some ambiguities in the formulation of the simple shear arising from the determination of the hydrostatic pressure p were highlighted by Horgan [24].

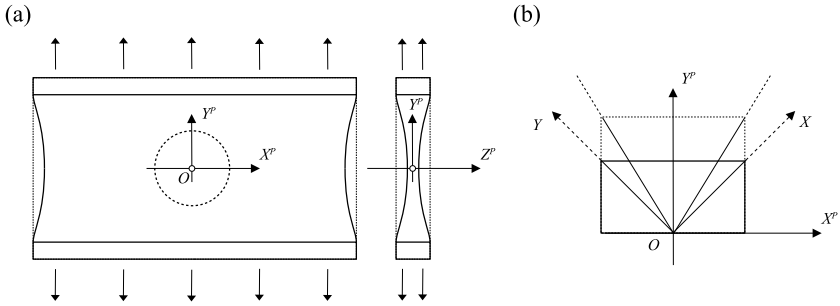

Fig. 3 Pure shear model of a plane rectangular sheet produced by the vertical extension of the clamped edges. Identification of the central area (a). Deformation of two inclined linear elements (b)

Cauchy stress tensor can be evaluated using (19) and it takes the following form:

$$[\mathbf{T}] = \begin{bmatrix} \mathrm{T}_{xx} & \mathrm{T}_{xy} & 0 \\ \mathrm{T}_{xy} & \mathrm{T}_{yy} & 0 \\ 0 & 0 & \mathrm{T}_{zz} \end{bmatrix}. \tag{26}$$

The comparison with the corresponding stress tensor (12) of the linear case shows that the simple shear in finite elasticity generates, in addition to the two tangential components, also of all three normal stress components.[13] These three diagonal component of $\mathbf{T}$ causes the loss of the pure shear stress condition defined in the linearized elasticity through form of the stress tensor (12). Destrade, Murphy and Saccomandi [26], to eliminate the three normal components of $\mathbf{T}$, suggest applying a state of triaxial extensions together with the simple shear.

To maintain the displacement field (9) in a sample it is necessary to apply, in its deformed configuration, the five stress components of the tensor (26).[14] It follows that, when the amount of shear k is large, the simple shear deformation is extremely difficult to replicate in the laboratory. This is the main reason why simple shear has little practical relevance, despite its historical derivation and conceptual significance.

3.2 Pure Shear Model

Pure shear model is achieved in a sheet under uniaxial extension. Such a deformation is obtained by stretching the sheet along the clamped edges, as shown in Fig. 3. Strictly speaking, the deformation takes the form of a pure shear only in the central part of the sheet since the lateral edges tend to curve and this effect propagates inwards to a certain extent [29, 36] and [38]. The reference system shown in Fig. 3a is principal. The deformation gradient with respect to it is

$$\left[\mathbf{F}^p\right] = \begin{bmatrix} 1 & 0 & 0 \\ 0 & \lambda_2 & 0 \\ 0 & 0 & \lambda_3 \end{bmatrix}. \tag{27}$$

[13] The property of unequal normal stresses $\mathrm{T}_{xx} \neq \mathrm{T}_{yy}$ in simple shear is referred to as the Poynting effect [25, 33] and [37].

[14] For a block of rubber subjected to simple shear, Rivlin [19] computed the normal and tangential surface tractions to apply to the inclined faces.

Unlike simple shear, for pure shear, area (being $da'/da = \lambda_2 \neq 1$) and volume (being $dv'/dv = \lambda_2\lambda_3 \neq 1$) change. As a particular case, the pure shear model allows analyzing incompressible deformations, in this case it is sufficient to assume: $\lambda_3 = 1/\lambda_2$. Figure 3b illustrates how two linear elements, positioned along the axes of a reference system rotated counterclockwise around the principal axis Z^p by an angle of $\pi/4$, undergo, due to the vertical extension, an angular distortion (as well as an elongation).

The deformation of the pure shear model, with respect to the rotated reference system (cf. Fig. 3b), is

$$\begin{cases} x = X + \frac{1}{2}(X+Y)(\lambda_2 - 1) \\ y = Y + \frac{1}{2}(X+Y)(\lambda_2 - 1) \\ z = \lambda_3 Z \end{cases} . \tag{28}$$

This deformation provides the following deformation gradient:[15]

$$[\mathbf{F}] = \begin{bmatrix} \frac{1}{2}(1+\lambda_2) & \frac{1}{2}(\lambda_2 - 1) & 0 \\ \frac{1}{2}(\lambda_2 - 1) & \frac{1}{2}(1+\lambda_2) & 0 \\ 0 & 0 & \lambda_3 \end{bmatrix} . \tag{29}$$

Even if generally it is not, for the pure shear, the tensor $\mathbf{F}$ is symmetric. Hence, from the polar decomposition theorem, $\mathbf{F} = \mathbf{RU}$, rigid rotations are absent, i.e. $\mathbf{R} = \mathbf{I}$ (namely, the pure shear deformation is irrotational), and the right stretch tensor coincides with the deformation gradient, i.e. $\mathbf{F} = \mathbf{U}$.

From the deformation gradient (29), the Green-St. Venant tensor $\mathbf{E}$ is directly obtained

$$[\mathbf{E}] = \frac{1}{2}\begin{bmatrix} \frac{1}{2}\left(\lambda_2^2 - 1\right) & \frac{1}{2}\left(\lambda_2^2 - 1\right) & 0 \\ \frac{1}{2}\left(\lambda_2^2 - 1\right) & \frac{1}{2}\left(\lambda_2^2 - 1\right) & 0 \\ 0 & 0 & \lambda_3^2 - 1 \end{bmatrix} . \tag{30}$$

Such a tensor contains the two shear strain components, $\mathrm{E}_{xy} = \mathrm{E}_{yx}$, but also two in-plane components, $\mathrm{E}_{xx} = \mathrm{E}_{yy}$, due to extensional deformations. In fact, the two material fibers, originally oriented along the X axis and Y axis (cf. Fig. 3b), are rotated and elongated. Therefore, also the pure shear model (as well as the simple shear model) produces combined angular and extensional deformation effects. Moreover, the two terms E_{xx} and E_{yy} cause the loss of the pure shear strain condition defined in the linearized elasticity through the form of the strain tensor $(10)_2$.

It is important to note that the Green-St. Venant tensor (30) is substantially different from the corresponding tensor (23).[16] *This means that the pure deformations, generated by simple*

[15] Alternatively, by imposing a rigid counterclockwise rotation of $\pi/4$ around the Z^p axis on the gradient deformation (27), the same tensor (29) is obtained ($\mathbf{F} = \mathbf{Q}^{\mathrm{T}}\mathbf{F}^p\mathbf{Q}$)

$$[\mathbf{F}] = \begin{bmatrix} \frac{\sqrt{2}}{2} & \frac{\sqrt{2}}{2} & 0 \\ -\frac{\sqrt{2}}{2} & \frac{\sqrt{2}}{2} & 0 \\ 0 & 0 & 1 \end{bmatrix}\begin{bmatrix} 1 & 0 & 0 \\ 0 & \lambda_2 & 0 \\ 0 & 0 & \lambda_3 \end{bmatrix}\begin{bmatrix} \frac{\sqrt{2}}{2} & -\frac{\sqrt{2}}{2} & 0 \\ \frac{\sqrt{2}}{2} & \frac{\sqrt{2}}{2} & 0 \\ 0 & 0 & 1 \end{bmatrix} =$$

$$\begin{bmatrix} \frac{1}{2}(1+\lambda_2) & \frac{1}{2}(\lambda_2 - 1) & 0 \\ \frac{1}{2}(\lambda_2 - 1) & \frac{1}{2}(1+\lambda_2) & 0 \\ 0 & 0 & \lambda_3 \end{bmatrix} .$$

[16] The two tensors are evaluated for the same reference system.

shear and pure shear models, are physically different. Consequently, in general, there is no possibility of applying a rigid rotation to the pure shear to obtain the simple shear (as instead happens in linearized elasticity).[17]

Using (30), formula (16) gives the sine of γ_{xy} for the pure shear model

$$\sin \gamma_{xy} = \frac{\lambda_2^2 - 1}{\lambda_2^2 + 1}. \tag{31}$$

The pure shear kinematics can be linearized by assuming: $\lambda_2 \simeq 1 + \varepsilon_2$, where the principal strain ε_2 is a (dimensionless) infinitesimal quantity. Then, ε_2^2 can be neglected, and the components of the tensor (30) reduces to: $\mathrm{E}_{xx} \simeq \varepsilon_2/2$, $\mathrm{E}_{yy} \simeq \varepsilon_2/2$ and $\mathrm{E}_{xy} \simeq \varepsilon_2/2 = \gamma_{xy}/2$. Substantially, (31) becomes $\sin \gamma_{xy} \simeq \gamma_{xy} = \varepsilon_2$. A rather surprising result is thus obtained. Once linearized, the pure shear model does not reproduce the corresponding case of linearized elasticity, illustrated by Fig. 1b.

Using, (18), (19) and (29), the Cauchy stress tensor for pure shear model can be determined. It takes the following form:

$$[\mathbf{T}] = \begin{bmatrix} \mathrm{T}_{xx} & \mathrm{T}_{xy} & 0 \\ \mathrm{T}_{xy} & \mathrm{T}_{xx} & 0 \\ 0 & 0 & \mathrm{T}_{zz} \end{bmatrix}. \tag{32}$$

As in the previous case of simple shear, also for the pure shear model, all three normal stress components are present in the stress tensor $\mathbf{T}$. Therefore, even for pure shear model, the pure shear stress condition defined in the linearized elasticity through the form of the stress tensor (12) is not verified.

The shear model of linearized elasticity as kinematic effect only considers the angular variation of two orthogonal material fibers, measured by the shear strain γ_{xy}. Differently, in the two shear models considered in this Section, the stress tensor $\mathbf{T}$ depends on the deformation gradient $\mathbf{F}$ (and on other tensors related to it), which describes, in a coupled way, the kinematic effects due to both angular variations and extensions of material fibres. This coupling can create uncertainties in constitutive modeling and generate difficulties in experimentally investigating the shear behavior of a material.

4 Purely Angular Shear in Finite Elasticity

As seen in the previous Sect. 3, the deformations provided by the simple and pure shear models in finite elasticity are *physically different*. Therefore, their adoption can lead to the formulation of constitutive laws or stored energy functions that do not provide the same material response. In addition, always in Sect. 3, some inadequacies for both shear models were highlighted, which effectively limit their application.

To overcome the critical issues, a new shear model is proposed below, which satisfies the following two basic requirements:

i. the shear model is based only on the angular variation of linear elements and not on their extension;

[17] Unfortunately, the contrary has been erroneously stated in many classical texts. For example, Treloar [38] (on page 85) "A simple shear is thus equivalent to a pure shear together with a rotation"; Love [39] (on page 71) "So that the simple shear is equivalent to a pure shear followed by a rotation through an angle α".

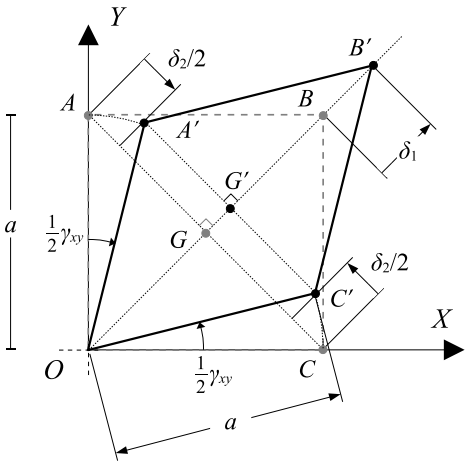

Fig. 4 Displacements in the XY plane. Geometric details of an angular shear deformation

ii. the linearization of the shear model must reproduce the corresponding shear model of the linearized elasticity.

The simple shear model of finite elasticity was conceived by Rivlin [19] on the basis of the analogous linearized elasticity model assuming that the only deformation parameter of this model, the amount of shear k, can be a finite quantity. More directly, one can refer to the pure shear model in linearized elasticity and assume that the shear strain γ_{xy}, defined as the variation of an initial right angle, can be large. With this assumption and the satisfaction of the two previous requirements, a new shear model in finite elasticity can be defined, which we will call *purely angular shear*.

Consider the cube with sides a and to illustrate the (plane) purely angular shear deformation, as previously done, refer to the cross section of the cube belonging to the XY plane. Similar to the case shown by Fig. 1b, this cross section (and all the sections parallel to it) is transformed into a rhombus (whose four sides are equal) by changing only the angle γ_{xy}, now of large magnitude.[18] Unlike pure shear strain treated in linearized elasticity, now the base section area, height and volume of the cube change with deformation.

The geometric details of a purely angular shear deformation are shown in Fig. 4. Unlike Fig. 1b, points A and C move in A' and C' along circular arcs with a radius equal to a. By introducing the displacements δ_1 and δ_2, shown in Fig. 4, and the uniform displacement δ_3 along the Z axis, the displacement field is

$$\begin{cases} u = \frac{\sqrt{2}}{4}\frac{1}{a}(X+Y)\,\delta_1 - \frac{\sqrt{2}}{4}\frac{1}{a}(X-Y)\,\delta_2 \\ v = \frac{\sqrt{2}}{4}\frac{1}{a}(X+Y)\,\delta_1 + \frac{\sqrt{2}}{4}\frac{1}{a}(X-Y)\,\delta_2 \\ w = \frac{Z}{a}\delta_3 \end{cases} . \tag{33}$$

The diagonals of the base section, AC and OB, remain orthogonal to each other after deformation. They are therefore principal directions. Using the principal stretches λ_1, λ_2 and λ_3, the displacements δ_1, δ_2 and δ_3 can be expressed as

$$\delta_1 = a\sqrt{2}\,(\lambda_1 - 1)\,, \quad \delta_2 = a\sqrt{2}\,(1-\lambda_2) \quad \text{and} \quad \delta_3 = a\,(\lambda_3 - 1)\,, \tag{34}$$

[18] However, due to the impenetrability of matter, the following inequalities must hold: $-\frac{3}{2}\pi < \gamma_{xy} < \frac{\pi}{2}$.

and the displacement field (33) transformed into

$$\begin{cases} u = -X + \frac{1}{2}(\lambda_1 + \lambda_2) X + \frac{1}{2}(\lambda_1 - \lambda_2) Y \\ v = -Y + \frac{1}{2}(\lambda_1 - \lambda_2) X + \frac{1}{2}(\lambda_1 + \lambda_2) Y \\ w = -Z + \lambda_3 Z \end{cases} . \tag{35}$$

Looking, for example, at the triangle $OA'G'$ of the deformed base section, we have: $OG' = a\frac{\sqrt{2}}{2}\lambda_1$, $A'G' = a\frac{\sqrt{2}}{2}\lambda_2$ and $OA' = a$, and from them a useful relationship between the stretches can be easily obtained

$$\frac{1}{2}\left(\lambda_1^2 + \lambda_2^2\right) = 1. \tag{36}$$

By calculating the gradient of the displacement field (35) and using (3), the deformation gradient is given by

$$[\mathbf{F}] = \begin{bmatrix} \frac{1}{2}(\lambda_1 + \lambda_2) & \frac{1}{2}(\lambda_1 - \lambda_2) & 0 \\ \frac{1}{2}(\lambda_1 - \lambda_2) & \frac{1}{2}(\lambda_1 + \lambda_2) & 0 \\ 0 & 0 & \lambda_3 \end{bmatrix}. \tag{37}$$

Since $\mathbf{F}$ is symmetric, then $\mathbf{R} = \mathbf{I}$ and $\mathbf{F} = \mathbf{U}$. The eigenvalues of the tensor $\mathbf{U}$ are the principal stretches λ_1, λ_2 and λ_3 already defined, as is easy to verify by solving the characteristic equation of $\mathbf{U}$.

Once the deformation gradient $\mathbf{F}$ is known, the Green-St. Venant tensor $\mathbf{E}$ can be determined

$$[\mathbf{E}] = \begin{bmatrix} 0 & \frac{1}{4}\left(\lambda_1^2 - \lambda_2^2\right) & 0 \\ \frac{1}{4}\left(\lambda_1^2 - \lambda_2^2\right) & 0 & 0 \\ 0 & 0 & \frac{1}{2}\left(\lambda_3^2 - 1\right) \end{bmatrix}. \tag{38}$$

Since the extensions along the X and Y axes are not occurring, the normal components E_{xx} and E_{yy}, unlike the simple and pure shear models (cf. (23) and (30)), are zero. Usually, in finite elasticity, in-plane deformation can generate out-of-plane deformation.[19] Thus, inevitably, the E_{zz} component also appears in $\mathbf{E}$.

For the purely angular shear model, the expression (16) of the shear deformation γ_{xy} reduces to $\left(\mathrm{E}_{xx} = \mathrm{E}_{yy} = 0\right)$

$$\sin\gamma_{xy} = 2\mathrm{E}_{xy} = \frac{\partial u}{\partial Y} + \frac{\partial v}{\partial X} + \left[\frac{\partial u}{\partial X}\frac{\partial u}{\partial Y} + \frac{\partial v}{\partial X}\frac{\partial v}{\partial Y} + \frac{\partial w}{\partial X}\frac{\partial w}{\partial Y}\right] = \frac{1}{2}\left(\lambda_1^2 - \lambda_2^2\right). \tag{39}$$

By linearizing (39), the terms in square brackets vanish and $\sin\gamma_{xy} \simeq \gamma_{xy}$, thus definition $(8)_1$ of the linearized elasticity is recovered.[20] Therefore, expression (39) can properly describe

[19] To avoid out-of-plane deformation, an orthogonal normal stress can be applied, but this in turn modifies the in-plane deformation.

[20] With the hypothesis of small deformations: $\lambda_1^2 \simeq 1 + 2\varepsilon_1$ and $\lambda_2^2 \simeq 1 + 2\varepsilon_2$, and being $\varepsilon_1 = -\varepsilon_2$ in the linearized pure shear, formula (39) gives

$$\frac{1}{2}\gamma_{xy} = \varepsilon_1.$$

(a) (b)

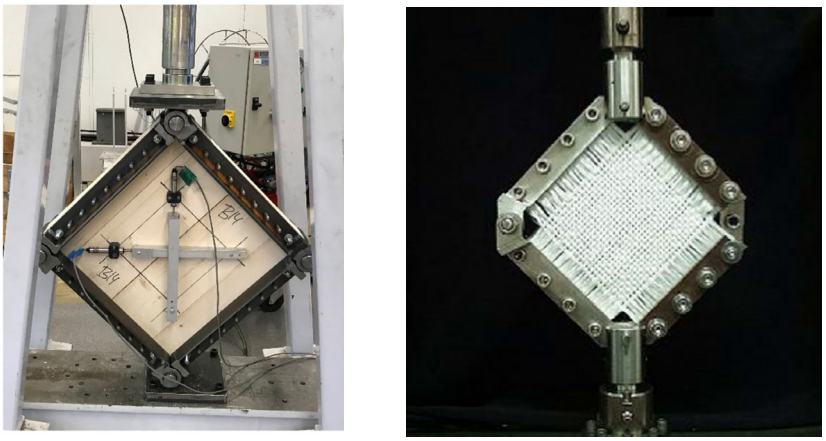

Fig. 5 Purely angular shear tests. Diagonal compression test [40](a). Picture frame test [41] (b)

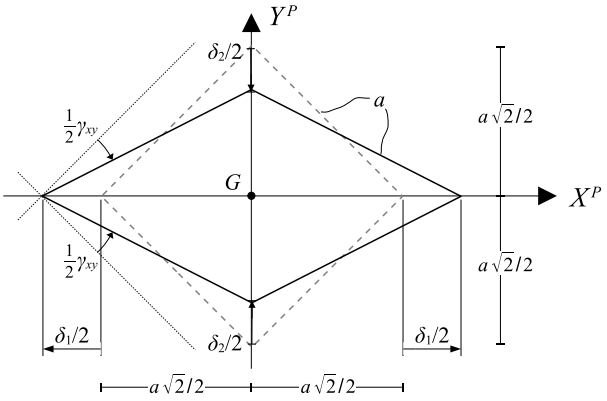

Fig. 6 Displacements with respect to the principal reference system

the "large/small" transition that the shear deformation γ_{xy} makes when passing from the nonlinear to the linearized elasticity.

For the purely angular shear model, the form of the Green-St. Venant tensor (38) is similar to that used in linearized elasticity to define the pure shear strain condition (cf. $(10)_2$), using only two components, $\mathrm{E}_{xy} = \mathrm{E}_{yx} = \frac{1}{2}\gamma_{xy}$, different from zero. In the tensor (38), given (39), the two non-zero off-diagonal components hold: $\mathrm{E}_{xy} = \mathrm{E}_{yx} = \frac{1}{2}\sin\gamma_{xy}$.

In some experimental analyses, so-called diagonal compression tests are envisaged. These are mechanical tests in which a sample is confined by stiffened beams connected at the ends by hinges, on which static forces are applied. As an example, Fig. 5a illustrates a diagonal compression test apparatus. Picture frame tests are similar experiments for characterize the material behavior of textile composites (see Fig. 5b).

The sample, in these tests, undergoes a deformation completely similar to that discussed up to this point. Figure 6 shows the geometric details to evaluate the displacement field with respect to the principal reference system, with origin in the centroid of the square and axes oriented according to the diagonals. Compared to the principal system, the displacement

field becomes

$$\begin{cases} u = \frac{X}{a\sqrt{2}}\delta_1 = -X + X\lambda_1 \\ v = -\frac{Y}{a\sqrt{2}}\delta_2 = -Y + Y\lambda_2 \\ w = \frac{Z}{a}\delta_3 = -Z + Z\lambda_3 \end{cases} . \tag{40}$$

To derive (40), (34) has been used. Obviously, system (40) is equivalent to (35), because it trivially describes the same transformation of the square into a rhombus. As is known, the representation of the displacement field in the principal system is the simplest, in particular the field is now decoupled, in the sense that u depends only on the variable X, etc. Consequently, the right stretch tensor $\mathbf{U}^p$ is diagonal[21]

$$[\mathbf{U}^p] = \begin{bmatrix} \lambda_1 & 0 & 0 \\ 0 & \lambda_2 & 0 \\ 0 & 0 & \lambda_3 \end{bmatrix} . \tag{41}$$

For the purely angular shear model, stretches λ_1 and λ_2 must be connected by relation (36). In this it differs transversally from a usual biaxial stretching problem, where these two stretches can be arbitrary.

Having discussed the kinematics of the angular shear model, we now move on to the evaluation of stress tensors with reference to the coordinate system of Fig. 4 and the deformation gradient (37). To use the constitutive law (18) it is necessary to previously evaluate the principal invariants of the Cauchy-Green tensors,

$$\begin{gathered} I_1 = 2 + \lambda_3^2, \\ I_2 = \lambda_1^2\lambda_2^2 + 2\lambda_3^2, \\ I_3 = \lambda_1^2\lambda_2^2\lambda_3^2, \end{gathered} \tag{42}$$

and the tensors $\mathbf{BF}$ and $\mathbf{F}^{-\mathrm{T}}$,

$$[\mathbf{BF}] = \begin{bmatrix} \frac{1}{2}(\lambda_1+\lambda_2)[2-\lambda_1\lambda_2] & \frac{1}{2}(\lambda_1-\lambda_2)[2+\lambda_1\lambda_2] & 0 \\ \frac{1}{2}(\lambda_1-\lambda_2)[2+\lambda_1\lambda_2] & \frac{1}{2}(\lambda_1+\lambda_2)[2-\lambda_1\lambda_2] & 0 \\ 0 & 0 & \lambda_3^3 \end{bmatrix}, \tag{43}$$

$$\left[\mathbf{F}^{-\mathrm{T}}\right] = \frac{1}{\lambda_1\lambda_2\lambda_3}\begin{bmatrix} \frac{1}{2}(\lambda_1+\lambda_2)\lambda_3 & -\frac{1}{2}(\lambda_1-\lambda_2)\lambda_3 & 0 \\ -\frac{1}{2}(\lambda_1-\lambda_2)\lambda_3 & \frac{1}{2}(\lambda_1+\lambda_2)\lambda_3 & 0 \\ 0 & 0 & \lambda_1\lambda_2 \end{bmatrix}. \tag{44}$$

[21] Obviously, by imposing on tensor (37) a rigid counterclockwise rotation of $\pi/4$ around the Z axis, the deformation gradient $\mathbf{F} = \mathbf{U}^p$, relating to the displacement field (40), is found again. This transformation can be represented as follows ($\mathbf{U}^p = \mathbf{Q}^{\mathrm{T}}\mathbf{U}\mathbf{Q}$):

$$\begin{aligned} \left[\mathbf{U}^p\right] &= \begin{bmatrix} \frac{\sqrt{2}}{2} & \frac{\sqrt{2}}{2} & 0 \\ -\frac{\sqrt{2}}{2} & \frac{\sqrt{2}}{2} & 0 \\ 0 & 0 & 1 \end{bmatrix}\begin{bmatrix} \frac{1}{2}(\lambda_1+\lambda_2) & \frac{1}{2}(\lambda_1-\lambda_2) & 0 \\ \frac{1}{2}(\lambda_1-\lambda_2) & \frac{1}{2}(\lambda_1+\lambda_2) & 0 \\ 0 & 0 & \lambda_3 \end{bmatrix}\begin{bmatrix} \frac{\sqrt{2}}{2} & -\frac{\sqrt{2}}{2} & 0 \\ \frac{\sqrt{2}}{2} & \frac{\sqrt{2}}{2} & 0 \\ 0 & 0 & 1 \end{bmatrix} \\ &= \begin{bmatrix} \lambda_1 & 0 & 0 \\ 0 & \lambda_2 & 0 \\ 0 & 0 & \lambda_3 \end{bmatrix}. \end{aligned}$$

The rigid translation of the reference system involves constants that are irrelevant in the computation of the deformation.

With (37), (42), (43) and (44), the constitutive law (18) provides the following Piola-Kirchhoff stress tensor:

$$[\mathbf{T}_R] = \begin{bmatrix} \mathrm{T}_{R_{xx}} & \mathrm{T}_{R_{xy}} & 0 \\ \mathrm{T}_{R_{xy}} & \mathrm{T}_{R_{xx}} & 0 \\ 0 & 0 & \mathrm{T}_{R_{zz}} \end{bmatrix}, \tag{45}$$

where

$$\mathrm{T}_{R_{xx}} = (\lambda_1 + \lambda_2)\left[\omega_{,1} + \left(\lambda_3^2 + \lambda_1\lambda_2\right)\omega_{,2} + \lambda_1\lambda_2\lambda_3^2\,\omega_{,3}\right],$$

$$\mathrm{T}_{R_{xy}} = (\lambda_1 - \lambda_2)\left[\omega_{,1} + \left(\lambda_3^2 - \lambda_1\lambda_2\right)\omega_{,2} - \lambda_1\lambda_2\lambda_3^2\,\omega_{,3}\right],$$

$$\mathrm{T}_{R_{zz}} = 2\lambda_3\left[\omega_{,1} + 2\omega_{,2} + \lambda_1^2\lambda_2^2\,\omega_{,3}\right],$$

with $\omega_{,i} = \frac{\partial \omega}{\partial I_i}$, for $i = 1, 2$ and 3. Since for the purely angular shear the tensors $\mathbf{F}$, $\mathbf{BF}$ and $\mathbf{F}^{-\mathrm{T}}$ are symmetric, then the Piola-Kirchhoff stress tensor $\mathbf{T}_R$ is also symmetric.

Using a Lagrangian analysis, it is easy to formulate the boundary value problem for the equilibrium of a cube subjected to a purely angular shear deformation. Being the deformation homogeneous, the stresses also do not vary. That is, these stresses are the same for every internal point of the cube and for its boundary. In particular, the stresses at the boundary can be interpreted as the external surface forces necessary to produce the displacement field (35).

In the undeformed configuration, equilibrium conditions require the following vectorial equation to be satisfied locally:

$$\mathrm{Div}\,\mathbf{T}_R + \mathbf{b} = \mathbf{o}, \tag{46}$$

where the symbol $\mathbf{b}$ denotes the body forces. The boundary conditions, to be added to the previous field equation, are

$$\mathbf{t}_R = \mathbf{T}_R\mathbf{n}, \tag{47}$$

where $\mathbf{t}_R$ denotes the Piola-Kirchhoff stress vector and $\mathbf{n}$ the outward unit normal. For the three faces of the cube with positive normal, (47) gives

$$[\mathbf{t}_R] = \begin{bmatrix} \mathrm{T}_{R_{xx}} \\ \mathrm{T}_{R_{xy}} \\ 0 \end{bmatrix}, \; [\mathbf{t}_R] = \begin{bmatrix} \mathrm{T}_{R_{xy}} \\ \mathrm{T}_{R_{xx}} \\ 0 \end{bmatrix}, \; [\mathbf{t}_R] = \begin{bmatrix} 0 \\ 0 \\ \mathrm{T}_{R_{zz}} \end{bmatrix}, \tag{48}$$

for $X = a$ and $0 \le Y, Z \le a$, $Y = a$ and $0 \le X, Z \le a$, $Z = a$ and $0 \le X, Y \le a$, respectively. For the three faces with negative normal, there are values opposite to the previous ones. By setting $\mathbf{b} = \mathbf{o}$, the three scalar differential equations given by (46) are automatically satisfied, because Piola-Kirchhoff stresses are constant. Based on the boundary conditions $(48)_{1,2}$, the normal stress component $\mathrm{T}_{R_{xx}}$ and the tangential stress component $\mathrm{T}_{R_{xy}}$ must be applied to the edges to obtain the deformation shown in Fig. 4. The third boundary condition $(48)_3$, relating to the two faces of the cube with normals parallel to the Z axis, can be used to impose the traction-free conditions for these two faces: $\mathrm{T}_{R_{zz}} = 0$, which provides an expression to calculate the principal stretch λ_3

$$\omega_{,1} + 2\omega_{,2} + \lambda_1^2\lambda_2^2\,\omega_{,3} = 0. \tag{49}$$

Using (37), (45) and (49), the formula (19) gives the Cauchy stress tensor

$$[\mathbf{T}] = \begin{bmatrix} \mathrm{T}_{xx} & \mathrm{T}_{xy} & 0 \\ \mathrm{T}_{xy} & \mathrm{T}_{xx} & 0 \\ 0 & 0 & 0 \end{bmatrix}, \tag{50}$$

with

$$\mathrm{T}_{xx} = \frac{2}{\lambda_1\lambda_2\lambda_3}\left[\omega_{,1} + \left(\lambda_1^2\lambda_2^2 + \lambda_3^2\right)\omega_{,2} + \lambda_1^2\lambda_2^2\lambda_3^2\,\omega_{,3}\right],$$

$$\mathrm{T}_{xy} = \frac{1}{\lambda_1\lambda_2\lambda_3}\left(\lambda_1^2 - \lambda_2^2\right)\left[\omega_{,1} + \lambda_3^2\,\omega_{,2}\right].$$

It can be observed that, to produce the finite purely angular shear deformation (38), it is always necessary to apply a equibiaxial normal stress T_{xx} in addition to the tangential stress T_{xy}.[22] Therefore, unlike linearized elasticity, *a state of pure shear deformation is not associated with a state of pure shear stress.*

Using the displacement field (40), obtained for the principal reference system, the tensors (43) and (44) take the diagonal form, and formula (18) yields the principal Piola-Kirchhoff stresses[23]

$$\left[\mathbf{T}_R^p\right] = \begin{bmatrix} \mathrm{T}^p_{R_{11}} & 0 & 0 \\ 0 & \mathrm{T}^p_{R_{22}} & 0 \\ 0 & 0 & \mathrm{T}^p_{R_{33}} \end{bmatrix}, \tag{51}$$

with

$$\mathrm{T}^p_{R_{11}} = 2\lambda_1\left[\omega_{,1} + 2\omega_{,2} + \lambda_3^2\omega_{,2} - \lambda_1^2\omega_{,2} + \lambda_2^2\lambda_3^2\,\omega_{,3}\right],$$

$$\mathrm{T}^p_{R_{22}} = 2\lambda_2\left[\omega_{,1} + 2\omega_{,2} + \lambda_3^2\omega_{,2} - \lambda_2^2\omega_{,2} + \lambda_1^2\lambda_3^2\,\omega_{,3}\right],$$

$$\mathrm{T}^p_{R_{33}} = 2\lambda_3\left[\omega_{,1} + 2\omega_{,2} + \lambda_1^2\lambda_2^2\,\omega_{,3}\right].$$

Obviously, the tangential stress components are zero and the third component is equal to $\mathrm{T}_{R_{zz}}$ in (45).

With the boundary condition (49), the above principal Piola-Kirchhoff stress components can be rewritten as follows:

$$\begin{cases} \mathrm{T}^p_{R_{11}} = 2\lambda_1\left(\lambda_3^2 - \lambda_1^2\right)\left[\omega_{,2} + \lambda_2^2\,\omega_{,3}\right] \\ \mathrm{T}^p_{R_{22}} = 2\lambda_2\left(\lambda_3^2 - \lambda_2^2\right)\left[\omega_{,2} + \lambda_1^2\,\omega_{,3}\right] \\ \mathrm{T}^p_{R_{33}} = 0 \end{cases}. \tag{52}$$

[22] Unlike simple shear model, for the purely angular shear model, the Poynting effect disappears.

[23] By imposing a rigid clockwise rotation of $\pi/4$ around the Z axis to the principal Piola-Kirchhoff stress tensor (51), the stress tensor (45) is recovered (that is, $\mathbf{T}_R = \mathbf{Q}\mathbf{T}^p_R\mathbf{Q}^{\mathrm{T}}$).

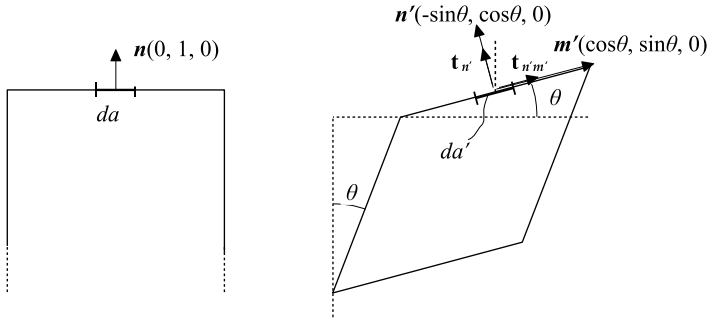

Fig. 7 Evaluation of normal and tangential Cauchy stress vector components along the upper face of the deformed cube

By applying the transformation (19) to (52), the principal Cauchy stresses are obtained[24]

$$\begin{cases} \mathrm{T}^p_{11} = \frac{2\lambda_1^2}{\lambda_1\lambda_2\lambda_3}\left(\lambda_3^2-\lambda_1^2\right)\left[\omega,_2 + \lambda_2^2\,\omega,_3\right] \\ \mathrm{T}^p_{22} = \frac{2\lambda_2^2}{\lambda_1\lambda_2\lambda_3}\left(\lambda_3^2-\lambda_2^2\right)\left[\omega,_2 + \lambda_1^2\,\omega,_3\right] \\ \mathrm{T}^p_{33} = 0 \end{cases} . \tag{53}$$

Once the stress tensor in the deformed configuration has been determined, the distribution of stresses present in the inclined faces of the deformed cube can be evaluated. The geometric shape of the deformed cube is described by the Eulerian coordinates (x, y, z), which are derived using (1) and the displacement field (35)

$$\begin{aligned} x &= \tfrac{1}{2}\left(\lambda_1+\lambda_2\right)X + \tfrac{1}{2}\left(\lambda_1-\lambda_2\right)Y \\ y &= \tfrac{1}{2}\left(\lambda_1-\lambda_2\right)X + \tfrac{1}{2}\left(\lambda_1+\lambda_2\right)Y \\ z &= \lambda_3 Z \end{aligned} . \tag{54}$$

We refer to the upper face of the deformed cube, the trace of which is illustrated in Fig. 7, since similar results are valid for the other three lateral faces. The unit vectors $\mathbf{n}'$ and $\mathbf{m}'$ of Fig. 7 have the following components: $\mathbf{n}' = (-\sin\theta, \cos\theta, 0)$ and $\mathbf{m}' = (\cos\theta, \sin\theta, 0)$, where $\theta = \frac{1}{2}\gamma_{xy}$, $\sin\theta = \frac{1}{2}\left(\lambda_1-\lambda_2\right)$ and $\cos\theta = \frac{1}{2}\left(\lambda_1+\lambda_2\right)$, and they are orthogonal to each other, that is $\mathbf{n}'\cdot\mathbf{m}' = 0$. With these unit vectors and the Cauchy stress tensor (50), the normal and tangential Cauchy stress vector components are calculated[25]

$$\mathrm{t}_{n'} = \mathbf{n}'\cdot\mathbf{T}\mathbf{n}' = \frac{2\lambda_1\lambda_2}{\lambda_3}\left(\omega,_1+\omega,_2\right) + 2\lambda_1\lambda_2\lambda_3\left(\omega,_2+\omega,_3\right), \tag{55}$$

[24] For the Cauchy stresses (50) and (53), a relation of the type $\mathbf{T} = \mathbf{Q}\mathbf{T}^p\mathbf{Q}^{\mathrm{T}}$ holds

$$[\mathbf{T}] = \begin{bmatrix} \frac{1}{2}\left(\mathrm{T}^p_{11}+\mathrm{T}^p_{22}\right) & \frac{1}{2}\left(\mathrm{T}^p_{11}-\mathrm{T}^p_{22}\right) & 0 \\ \frac{1}{2}\left(\mathrm{T}^p_{11}-\mathrm{T}^p_{22}\right) & \frac{1}{2}\left(\mathrm{T}^p_{11}+\mathrm{T}^p_{22}\right) & 0 \\ 0 & 0 & 0 \end{bmatrix}.$$

By introducing stress components (53) into this tensor, stress tensor (50) is found again.

[25] By multiplying $\mathrm{t}_{n'}$ and $\mathrm{t}_{n'm'}$ by $\lambda_3 a^2$ it is immediate to obtain the normal force and the shear force acting on the inclined faces.

$$\mathrm{t}_{n'm'} = \mathbf{m}' \cdot \mathbf{T}\mathbf{n}' = \frac{\left(\lambda_1^2 - \lambda_2^2\right)}{\lambda_3} \left(\omega_{,1} + \lambda_3^2 \omega_{,2}\right). \tag{56}$$

Excluding the infinitesimal case shown in Fig. 1b, where $\gamma_{xy} \simeq \mathcal{O}(\theta)$, for a generic expression of the stored energy function ω, there are no plausible reasons to presume $\mathrm{t}_{n'} = 0$. That is, in general, normal stress accompanies tangential stress.

In Appendix A, an application of the Mohr's circle to the plane stresses obtained for the purely angular shear model is reported.

In Appendix B, through the linearization of the principal formulae obtained in this Section for the purely angular shear model, the classic results of the infinitesimal elasticity for the pure shear are found.

5 Applications

In the previous Sections, the expression of the stored energy function ω was kept completely arbitrary. In the following, to be able to perform numerical applications, it is necessary to assign the form of ω. For it the compressible Mooney-Rivlin law is assumed[26,27]

$$\omega(I_1, I_2, I_3) = \bar{a} I_1 + b I_2 + c I_3 - (\bar{a} + 2b + c) \ln I_3, \tag{57}$$

where the constants $\bar{a}$, b and c are strictly positive quantities. It is well known that the above stored energy function, which depends on all three deformation invariants, describes properly the constitutive behavior of rubbers and rubber-like materials. From (57), the following derivatives can be computed:

$$\omega_{,1} = \bar{a}, \quad \omega_{,2} = b, \quad \omega_{,3} = c - \frac{\bar{a} + 2b + c}{I_3}, \tag{58}$$

where $\omega_{,i} = \frac{\partial \omega}{\partial I_i}$, for $i = 1$, 2 and 3. With these three derivatives, the stress components (45) become

$$\begin{aligned} \mathrm{T}_{R_{xx}} &= (\lambda_1 + \lambda_2)\left[\left(1 - \tfrac{1}{\lambda_1\lambda_2}\right)\bar{a} + \left(\lambda_3^2 + \lambda_1\lambda_2 - \tfrac{2}{\lambda_1\lambda_2}\right) b + \left(\lambda_1\lambda_2\lambda_3^2 - \tfrac{1}{\lambda_1\lambda_2}\right) c\right], \\ \mathrm{T}_{R_{xy}} &= (\lambda_1 - \lambda_2)\left[\left(1 + \tfrac{1}{\lambda_1\lambda_2}\right)\bar{a} + \left(\lambda_3^2 - \lambda_1\lambda_2 + \tfrac{2}{\lambda_1\lambda_2}\right) b + \left(\tfrac{1}{\lambda_1\lambda_2} - \lambda_1\lambda_2\lambda_3^2\right) c\right], \end{aligned} \tag{59}$$

while condition (49) provides

$$\lambda_3 = \sqrt{\frac{\bar{a} + 2b + c}{\bar{a} + 2b + \lambda_1^2\lambda_2^2 c}}. \tag{60}$$

To evaluate the normal and tangential stresses acting on the deformed faces of the cube we use (55) and (56), which for a compressible Mooney-Rivlin material take the following form:

$$\mathrm{t}_{n'} = \frac{2}{\lambda_3}\left[\left(\lambda_1\lambda_2 - \frac{1}{\lambda_1\lambda_2}\right)\bar{a} + \left(\lambda_1\lambda_2 + \lambda_1\lambda_2\lambda_3^2 - \frac{2}{\lambda_1\lambda_2}\right) b + \left(\lambda_1\lambda_2\lambda_3^2 - \frac{1}{\lambda_1\lambda_2}\right) c\right], \tag{61}$$

[26] This function is polyconvex and satisfies the growth conditions: $\omega \to \infty$ as $\lambda \to 0^+$ or $\lambda \to +\infty$. It was used, for example, in [42–44] and [45].

[27] For an extensive discussion of the terms related to the volume change in the stored energy function see the recent paper by M. Pelliciari et al. [46].

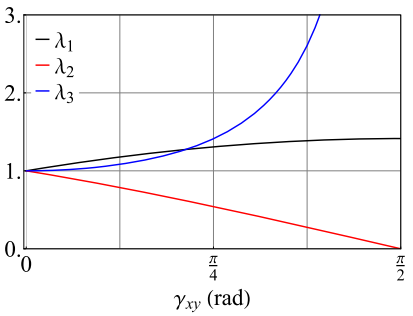

Fig. 8 Principal stretches λ_i versus the shear angle γ_{xy}

$$\mathrm{t}_{n'm'} = \frac{\left(\lambda_1^2 - \lambda_2^2\right)}{\lambda_3}\left(\bar{a} + \lambda_3^2 b\right). \tag{62}$$

Note that, by virtue of the normalization carried out on the shape of the energy (57), in the absence of deformation, $\lambda_1 = \lambda_2 = \lambda_3 = 1$, all the stresses (59), (61) and (62) vanish.

For the constitutive parameters, the following values are assumed: $\bar{a} = 19.43$, $b = 7.25$ and $c = 79.799$ kPa, which have been estimated experimentally by the authors for specimens performed using the silicone rubber Dragon Skin FX Pro and subjected to uniaxial tension and compression, torsion and unequal biaxial loading [47] and [48].

Figure 8 shows the values of the principal stretches λ_i as a function of the shear angle γ_{xy}. The stretch λ_1 occurs along the bisector of the square displayed in Fig. 4, or, similarly, along the horizontal axis of the principal system drawn in Fig. 6. The stretch λ_1 describes a monotonically increasing extension with the shear angle γ_{xy}, which varies in the range $[0, \pi/2)$. This stretch, whose values belong to the interval $[1, \sqrt{2})$, grows more rapidly in the first part of the plot and then reaches the (unrealistic) limit value $\sqrt{2}$, for which an *extreme deformation* occurs (the area of the initial square ideally collapses into a segment of length $2a$).[28] Orthogonal to λ_1, the in-plane stretch λ_2 describes a monotonically increasing contraction. This stretch belongs to the interval $[1, 0)$. As γ_{xy} increases, the deviation (in absolute value) from the unit value is greater for λ_2 than for λ_1.[29] The out-of-plane stretch λ_3 describes a monotonically increasing extension. This stretch starts with a unit value and horizontal slope[30] and grows weakly in the initial part of the graph and then rises sharply, highlighting a strong transversal dilation of the cube for large values of γ_{xy}.[31]

[28] This deformation requires unlimited energy.

[29] This is because the stretch λ_2 governs a transformation that reduces the initial segment of length $a\sqrt{2}$ to zero, while the stretch λ_1 describes the deformation that transforms the initial segment still of length $a\sqrt{2}$ to the final segment of length $2a$.

[30] In linearized elasticity, no transverse deformation occurs, $\lambda_3 = 1$ or $\varepsilon_z = 0$.

[31] In Fig. 8, the intersection point $\lambda_3 = \lambda_1 = \bar{\lambda}_{13}$, between the stretch curves λ_3 and λ_1, can be obtained using (36) and (60) and evaluating the only admissible root

$$\bar{\lambda}_{13} = \sqrt{\frac{1}{2}\left(1 + \sqrt{\frac{4\bar{a} + 8b + 5c}{c}}\right)}.$$

For $c \to \infty$ the material becomes incompressible and above root expression becomes $\bar{\lambda}_{13} = \sqrt{\frac{1}{2}\left(1 + \sqrt{5}\right)}$.

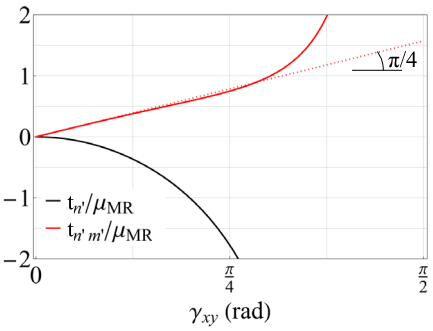

Fig. 9 Cauchy stress vector components normalized with respect to the linearised shear modulus μ_{MR}

Figure 9 shows the normal and tangential components of the Cauchy stress vector (55) and (56), that is the stresses that arise on the inclined faces of the deformed cube as the shear angle γ_{xy} increases. These stresses are normalized with respect to the linearized shear modulus of the Mooney-Rivlin material $\mu_{MR} = 2(\bar{a} + b)$ [42]. The tangential component $t_{n'm'}$, which occurs in the same direction as γ_{xy} (or, similarly, that does positive work for γ_{xy}), initially has a linear trend (as happens in the linearized theory) and then grows rapidly when γ_{xy} becomes large, denoting a strong nonlinear behavior. Given the normalization, the slope of the initial section of the curve is unity. The normal component $t_{n'}$ is compressive, it starts from zero with zero slope (as happens in linearized elasticity) and grows rapidly with γ_{xy}. Except in the initial part of the graph, the normal component $t_{n'}$ is, in absolute value, greater than the corresponding tangential component $t_{n'm'}$.

Figure 9 further highlights that, in finite elasticity, to generate a shear angle γ_{xy} it is necessary to apply in the xy plane both shear and normal stresses.

6 Conclusions

In this paper the large shear deformation of hyperelastic, isotropic, compressible materials has been investigated from a continuum mechanics standpoint.

The two most popular models, simple shear and pure shear models, not only do not differ by a rigid rotation (as occurs in linearized elasticity), but are actually physically different. The deformation field of the simple shear model (applied to the XY plane) has a similar form to that of the linearized elasticity, with the only difference that the amount of shear k is now assumed to be large. The resulting deformation preserves area and volume. Therefore, simple shear model can only be used for incompressible materials. The corresponding Green-St. Venant tensor, in addition to the shear components $E_{xy} = E_{yx}$, also contains the normal component E_{yy}, which shows how, due to the nonlinearities, also extensions of the material fibers along Y arise.

Pure shear model is achieved by subjecting a sheet to uniaxial extension. The deformation is measured with respect to a reference system rotated by $\pi/4$ with respect to the direction of extension. The corresponding Green-St. Venant tensor, in addition to the shear components $E_{xy} = E_{yx}$, also contains the normal components $E_{xx} = E_{yy}$ and E_{zz}, showing how in the pure shear model also arise the extensions of the material fibers along three directions X, Y and Z.

The pure shear condition, defined in linearized elasticity through the particular form of the strain tensor, which has only the two shear components other than zero, is lost in the case of simple shear when moving to finite elasticity. In fact, the Green-St. Venant tensor, which

represents the extension of the strain tensor to finite elasticity, also has a normal component. The same happens for pure shear model.

Two more drawbacks of the classic shear models can be highlighted. In practice, the simple shear model is difficult to use for experimental tests. In fact, to maintain the deformation of this model, five stress fields must be applied to the sample. Once linearized, the pure shear model does not reproduce the corresponding case of the linearized elasticity, because the in-plane components $\mathrm{E}_{xx} = \mathrm{E}_{yy}$ do not cancel.

In any case, the main difficulty encountered with the two classical shear models lies in the fact that both generate kinematic effects due to angular distortions but also to extension deformations. This coupling can create uncertainties in constitutive modeling and generate difficulties in investigating the shear behavior of a material.

With the purpose of evaluating the shear response function for hyperelastic, isotropic and compressible materials, the purely angular shear model has been proposed in this paper. As conceived for the nonlinear extension of the simple shear, the pure shear of the linearized elasticity has been generalized by supposing that the shear strains can become large. The purely angular shear model is based only on the angular variation of linear elements and not on their extension. The purely angular shear model applied to a cube transforms the base cross section, for example belonging to the *XY* plane, into a rhombus (whose four sides are equal) by changing only the angle γ_{xy}, now of large magnitude. Unlike linearized pure shear, now the base cross section, height and volume of the cube change with deformation.

For the purely angular shear model, the displacement field, deformation gradient and Green-St. Venant tensor for large shear deformation have been determined. In particular, unlike the two classic nonlinear shear models, the Green-St. Venant tensor has a form similar to the infinitesimal shear strain tensor, with the two shear components $\mathrm{E}_{xy} = \mathrm{E}_{yx} = \frac{1}{2}\sin\gamma_{xy}$ different from zero, and all the others equal to zero, with the exception of the normal component E_{zz} (which inevitably is different from zero because of the orthogonal deformation to the *XY* plane).

By representing the purely angular shear model in the principal reference system, the typical displacement field of some well-known experimental tests, for example the diagonal compression test and the picture frame test, are obtained.

Using a Lagrangian analysis, the boundary value problem for the equilibrium of a cube subjected to purely angular shear has been formulated. In this way, Piola-Kirchhoff and Cauchy stress fields were evaluated. The determination of the stress fields highlighted that to produce a finite angular shear deformation it is always necessary to apply an equibiaxial normal stress $\mathrm{T}_{xx} = \mathrm{T}_{yy}$ in addition to the tangential stress T_{xy}. Therefore, unlike linearized elasticity, a state of pure shear deformation is not associated with a state of pure shear stress. The normal and tangential Cauchy stress vector components on the inclined faces of the deformed cube have been calculated.

In the analyses, the stored energy function was never specified, so that the results obtained are valid for any hyperelastic, isotropic and compressible material.

To perform numerical applications, the compressible Mooney-Rivlin law has been assigned to the stored energy function. Numerical solutions has been obtained for the three principal stretches as of the shear angle $\gamma_{xy} \in [0, \pi/2)$ varies. Similarly, the normal and the tangential components of the Cauchy stress vector, acting on the inclined faces of the deformed cube, have been computed. After the initial phase, this application has shown that the normal component, in absolute value, becomes greater than the associated tangential component.

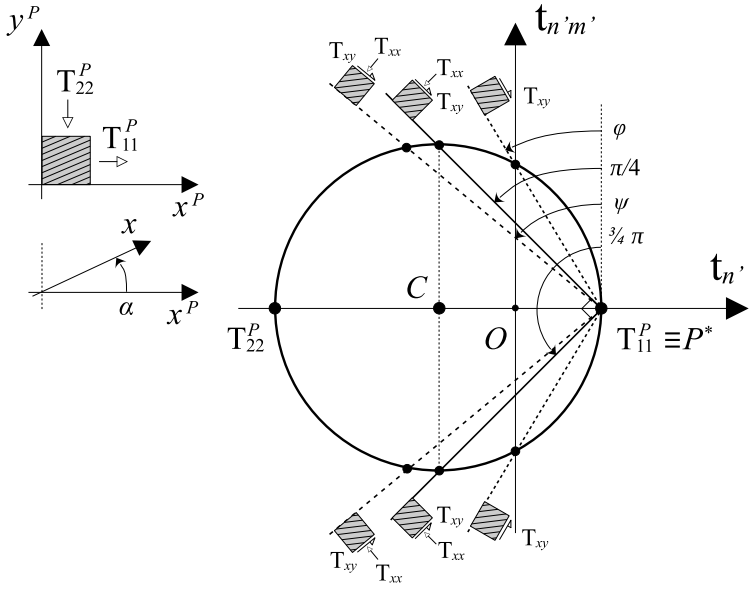

Fig. 10 Mohr's circle related to Cauchy stresses

Appendix A: Mohr's Circle of the Purely Angular Shear Stresses

In this Appendix A, an application of the Mohr's circle to the plane principal stresses (53), derived from the purely angular shear model, is performed. This geometric construction is equivalent to placing oneself at the origin of the principal reference system in Fig. 6 and evaluating the stress pair $(\mathrm{t}_{n'}, \mathrm{t}_{n'm'})$ for each direction exiting from this point. Although no constitutive prescription has been formalized in Sect. 4, we assume on a purely qualitative level that: $\mathrm{T}^p_{11} > 0$, $\mathrm{T}^p_{22} < 0$ and $\left|\mathrm{T}^p_{22}\right| > \mathrm{T}^p_{11}$. Figure 10 shows the Mohr's circle drawn starting from (53). The two solid half-lines identify the directions along which the tangential stress is maximum. These two directions are orthogonal to each other and form angles of $\frac{\pi}{4}$ and $\frac{3}{4}\pi$ with respect to the principal axis x^p. In absolute value, the maximum of the tangential stresses is equal to the radius of the circle: $\mathrm{T}_{xy} = \frac{1}{2}\left(\mathrm{T}^p_{11} - \mathrm{T}^p_{22}\right)$. Along these two directions, the tangential stresses are associated with the same normal stress, whose value is equal to the abscissa of the center of the circle: $\mathrm{T}_{xx} = \frac{1}{2}\left(\mathrm{T}^p_{11} + \mathrm{T}^p_{22}\right)$. The results relating to these two directions coincide with those already obtained previously (cf. footnote 24 and (50)).

There are two directions, highlighted in Mohr's circle with dotted half-lines, not orthogonal to each other, along which there is only tangential stress. They are identified by the two angles φ and $\pi - \varphi$. Each point of the Mohr's circle has a one-to-one correspondence with the stress values given by the following two expressions:

$$\begin{cases} \mathrm{t}_{n'} = \mathrm{T}^p_{11}\cos^2\alpha + \mathrm{T}^p_{22}\sin^2\alpha \\ \mathrm{t}_{n'm'} = -\mathrm{T}^p_{11}\sin\alpha\,\cos\alpha + \mathrm{T}^p_{22}\sin\alpha\,\cos\alpha \end{cases}, \tag{63}$$

where α is the angle indicated on the left side of Fig. 10. Therefore, by imposing $t_{n'} = 0$ and using (36), (49), (53) and $(63)_1$, the following expression for the angle φ is obtained:

$$\sin\varphi = \sqrt{\frac{\lambda_1^2\left(\lambda_3^2-\lambda_1^2\right)\left[\omega,_2+\lambda_2^2\,\omega,_3\right]}{\left(\lambda_1^2-\lambda_2^2\right)\left[\omega,_1+\lambda_3^2\,\omega,_2\right]}}. \tag{64}$$

Then introducing the values of φ and $\pi-\varphi$ into $(63)_2$ we obtain the corresponding values of the tangential stresses (i.e. the points of intersection of the two dotted half-lines with the circle).

The normal direction to the inclined face of the first quadrant of Fig. 6 forms an angle $\psi = \frac{\pi}{4} + \frac{\gamma_{xy}}{2}$ with the x^p axis. The normal of the second quadrant forms the angle $\pi - \psi$. These two directions, highlighted in Mohr's circle of Fig. 10 with dashed half-lines, are not orthogonal to each other. The normal to the first quadrant is represented by the following unit vector: $\mathbf{n}' = (\cos\psi, \sin\psi, 0)$, where $\cos\psi = \frac{\sqrt{2}}{2}\lambda_2$ and $\sin\psi = \frac{\sqrt{2}}{2}\lambda_1$. Using (63), together with (36), (49) and (53), the normal and tangential stresses along this direction can be evaluated (upper intersection point). Instead, for the normal of the second quadrant, $\mathbf{n}' = (-\cos\psi, \sin\psi, 0)$, formulae (55) and (56) (bottom intersection point), derived in the study of the case illustrated in Fig. 7, are obtained again.

Appendix B: Linearization of the Purely Angular Shear Model

Invoking the hypothesis of smallness of both the deformation and displacement fields, the nonlinear mathematical formulation presented in the Sect. 4 for the purely angular shear will be linearized, retrieving the classic results of linear theory. In particular, the angle γ_{xy} is supposed to be a very small quantity, so that its tangent can be confused with it (i.e., $\tan\gamma_{xy} \simeq \gamma_{xy} + o\left(\gamma_{xy}\right)$).[32] Therefore, with reference to Fig. 4, it follows that

$$\delta_1 = \delta_2 \simeq a\frac{\sqrt{2}}{2}\gamma_{xy} + o\left(\gamma_{xy}\right), \qquad \delta_3 \simeq o\left(\gamma_{xy}\right). \tag{65}$$

With these displacements, the principal stretches become[33]

$$\lambda_1 = 1 + \frac{1}{2}\gamma_{xy}, \quad \lambda_2 = 1 - \frac{1}{2}\gamma_{xy}, \quad \lambda_3 = 1. \tag{66}$$

Substituting (66) in (35), the displacement field for the purely angular shear reduces to

$$\begin{cases} u = \frac{1}{2}\gamma_{xy}Y \\ v = \frac{1}{2}\gamma_{xy}X \\ w = o \end{cases}, \tag{67}$$

coinciding with the displacement field of the linearized elasticity for the pure shear strain, as represented in Fig. 1b. Being $\frac{1}{2}\left(\lambda_1^2-\lambda_2^2\right) \simeq \gamma_{xy}$, the linearization of the Green-St. Venant tensor (38) leads directly to the infinitesimal strain tensor $(10)_2$. This is important for describing the deformation during the large/small transition. The relation (36),

[32] The Landau symbol was used.

[33] In the following, the infinitesimals of higher order will be omitted.

being $\frac{1}{2}\left(\lambda_1^2+\lambda_2^2\right)\simeq 1$, transforms into an identity, therefore, in linearized elasticity, it always results satisfied. The linearization of (39) also provides an identity ($\sin\gamma_{xy}\simeq\gamma_{xy}$ and $\frac{1}{2}\left(\lambda_1^2-\lambda_2^2\right)\simeq\gamma_{xy}$).

Using (66), the invariants (42) assume the following values:

$$I_1=I_2\simeq 3,\quad I_3\simeq 1, \tag{68}$$

showing how in linearized elasticity there are no variations in area and volume.

Using (66), the linearized forms of the tensors (37), (43) and (44) are obtained. Introducing these tensors, together with (68), into (45) the linearized expressions of the non-zero components of the Piola-Kirchhoff stress tensor are computed

$$\mathrm{T}_{R_{xx}}=\mathrm{T}_{R_{zz}}=2\left(\omega_{,1}+2\omega_{,2}+\omega_{,3}\right) \tag{69}$$

$$\mathrm{T}_{R_{xy}}=\gamma_{xy}\left(\omega_{,1}-\omega_{,3}\right).$$

Condition (49), which prescribes zero stresses in the two faces of the cube with normals parallel to the Z axis, simplifies in

$$\omega_{,1}+2\omega_{,2}+\omega_{,3}=0. \tag{70}$$

Given (70), the normal stresses $(69)_1$ vanish and the shear stress $(69)_2$ becomes

$$\mathrm{T}_{R_{xy}}=2\gamma_{xy}\left(\omega_{,1}+\omega_{,2}\right). \tag{71}$$

The linearization of the Cauchy stress tensor (51) provides

$$\mathrm{T}_{xx}=0,\quad \mathrm{T}_{xy}=2\gamma_{xy}\left(\omega_{,1}+\omega_{,2}\right), \tag{72}$$

showing, as is well known in linearized elasticity, that the two stress measures coincide.

For Mooney-Rivlin materials at small deformations, the shear modulus of elasticity is $\mu_{MR}=2(\bar{a}+b)$ [42], and from (72) the classical form of linearized shear stress is obtained

$$\mathrm{T}_{xy}=\mu_{MR}\,\gamma_{xy}. \tag{73}$$

Author Contributions F.O.F.: Experimental conceptualization, investigation, software, validation. L.L.: data reduction, investigation, writing – review. A.M.T.: visualization, supervision, project administration, funding acquisition.

Funding Information Open access funding provided by Università degli Studi di Modena e Reggio Emilia within the CRUI-CARE Agreement. Financial support from the Italian Ministry of University and Research (MUR) through the research project FISA-2022-00183 "Earth-Tech" - Implementation of new Shot-Earth technology in the construction industry, CUP: E93C24000250001, and project PRIN2022PNRR "New challenges of thin-walled structures at large strains and their promising applications" (prot. P2022AHFCP; CUP: C53D23008220001) are gratefully acknowledged.

Data Availability No datasets were generated or analysed during the current study.

Declarations

Competing Interests The authors declare no competing interests.

References

1. Rouse Ball, W.W.: A Short Account of the History of Mathematics. Macmillan, London (1908)
2. Rice, J.R.: Solid Mechanics. Harvard University (2010)
3. Parents, A.: Essais et recherches de mathematique et de physique. J. de Nully (1713)
4. Coulomb, C.A.: Essai sur une application des règles de maximis et minimis à quelques problèmes de statique, relatifs à l'architecture. Mém. Divers Savants **7**, 343–382 (1773)
5. Cauchy, A.-L.: Recherches sur l'équilibre et le mouvement intérieur des corps solides ou fluides, élastiques ou non élastiques. Bull. Soc. Philomath. **9–13** (1823)
6. Cauchy, A.-L.: De la pression ou tension dans un corps solide. Exerc. Math. **2**, 42–56 (1827)
7. Cauchy, A.-L.: Sur les pressions ou tensions supportées en un point donné d'un corps solide par trois plans perpendiculaires entre eux. Exerc. Math. **4**, 30–40 (1829)
8. Cauchy, A.-L.: Mémoire sur !es dilatations, les condensations et les rotations produits par un changement de forme dans un système de points matériels. Exerc. Phys. Math. **2**, 302–330 (1841)
10. Ericksen, J.L.: Appendix. Tensor fields. In: Flügge, S. (ed.) Handbuch der Physik III/1, pp. 794–858. Springer, Berlin (1960)
11. Boulanger, P., Hayes, M.: On shearing, stretching and spin. Theor. Comput. Fluid Dyn. **15**(4), 199–229 (2002)
12. Boulanger, P., Hayes, M.: A note on maximum shear. J. Elast. **69**(1), 215–222 (2002)
13. Boulanger, P., Hayes, M.: On pure shear. J. Elast. **77**(1), 83–89 (2004)
14. Boulanger, P., Hayes, M.: Constructions of unsheared pairs in finite strain. Int. J. Non-Linear Mech. **40**(2–3), 289–293 (2005)
15. Boulanger, P., Hayes, M.: Consequences of a result on pure shear. Int. J. Non-Linear Mech. **42**(2), 376–380 (2007)
16. Boulanger, P., Hayes, M.: Determination of the infinitesimal strain tensor from shears and elongations. J. Elast. **92**(3), 209–216 (2008)
17. Boulanger, P., Hayes, M.: Determination and factorization of the Cauchy–Green strain tensors from shears and stretches. Int. J. Eng. Sci. **47**(11–12), 1119–1130 (2009)
18. Boulanger, P., Hayes, M.: Using an unsheared pair to construct the strain ellipse. Math. Mech. Solids **16**(7), 739–752 (2011)
19. Rivlin, R.S.: Large elastic deformation of isotropic materials. IV. Further developments of the general theory. Philos. Trans. R. Soc. A **241**, 379–397 (1948)
20. Mooney, M.: Stress-strain curves of rubbers in simple shear. J. Appl. Phys. **35**, 23–26 (1944)
21. Brown, R.: Physical Testing of Rubber. Springer, New York (2006)
22. Truesdell, C.: The Elements of Continuum Mechanics. University Press, Cambridge (2008)
23. Moon, H., Truesdell, C.: Interpretation of adscititious inequalities through the effects pure shear stress produces upon an isotropic elastic solid. Arch. Ration. Mech. Anal. **55**, 1–17 (1974)
24. Horgan, C.O., Murphy, J.G.: Simple shearing of incompressible and slightly compressible isotropic nonlinearly elastic materials. J. Elast. **98**, 205–221 (2010)
25. Mihai, L.A., Goriely, A.: Numerical simulation of shear and Poynting effects by finite element method: an application of the generalised empirical inequalities in non-linear elasticity. Int. J. Non-Linear Mech. **49**, 1–14 (2013)
26. Destrade, M., Murphy, J.G., Saccomandi, G.: Simple shear is not so simple. Int. J. Non-Linear Mech. **47**, 210–214 (2012)
27. Thiel, C., Voss, J., Martin, R.J., Neff, P.: Shear, pure and simple. Int. J. Non-Linear Mech. **49**, 57–72 (2019)
28. Treloar, L.R.G.: Stress-strain data for vulcanised rubber under various types of deformation. Trans. Faraday Soc. **40**, 59–70 (1944)
29. Rivlin, R.S., Saunders, D.W.: Large elastic deformations of isotropic materials VII. Experiments on the deformation of rubber. Philos. Trans. R. Soc. A **243**, 251–288 (1951)

30. Sasso, M., Palmieri, G., Chiappini, G., Amodio, D.: Characterization of hyperelastic rubber-like materials by biaxial and uniaxial stretching tests based on optical methods. Polym. Test. **27**, 995–1004 (2008)
31. Segal, V.M.: Severe plastic deformation: simple shear versus pure shear. Mater. Sci. Eng. A **338**, 331–344 (2002)
32. Moreira, D.C., Nunes, L.C.S.: Comparison of simple and pure shear for an incompressible isotropic hyperelastic material under large deformation. Polym. Test. **32**, 240–248 (2013)
33. Truesdell, C., Noll, W.: The Non-linear Field Theories of Mechanics, 2nd edn. Springer, Berlin (1965)
34. Pardis, N., Ebrahimi, R., Kim, H.S.: Equivalent strain at large shear deformation: theoretical, numerical and finite element analysis. J. Appl. Res. Technol. **15**, 442–448 (2017)
9. Boulanger, P., Hayes, M.: On the finite shear. Arch. Ration. Mech. Anal. **151**, 125–185 (2000)
35. Green, A.E., Zerna, W.: Theoretical Elasticity, 2nd edn. Clarendon, Oxford (1968)
36. Ogden, R.W.: Nonlinear Elastic Deformations. Ellis Horwood, Chichester (1984). Reprinted by Dover, New York (1997)
37. Gurtin, M.E., Fried, E., Anand, L.: The Mechanics and Thermodynamics of Continua. Cambridge University Press, Cambridge (2010)
38. Treloar, L.R.G.: The Physics of Rubber Elasticity. Clarendon, Oxford (1975)
39. Love, A.E.H.: A Treatise on the Mathematical Theory of Elasticity. Dover, New York (1944)
40. Turesson, J., Björnfot, A., Berg, S., Ekevad, M., Tomasi, R.: Picture frame and diagonal compression testing of cross-laminated timber. Mater. Struct. **52**, 66 (2019). https://doi.org/10.1617/s11527-019-1372-7
41. Zhu, B., Yu, T.X., Tao, X.M.: An experimental study of in-plane large shear deformation of woven fabric composite. Compos. Sci. Technol. **67**, 252–261 (2007)
42. Lanzoni, L., Tarantino, A.M.: Finite anticlastic bending of hyperelastic solids and beams. J. Elast. **131**, 137–170 (2018)
43. Lanzoni, L., Tarantino, A.M.: The bending of beams in finite elasticity. J. Elast. **139**, 91–121 (2020)
44. Lanzoni, L., Tarantino, A.M.: Mechanics of high-flexible beams under live loads. J. Elast. **140**, 95–125 (2020)
45. Falope, F.O., Lanzoni, L., Tarantino, A.M.: The bending of fully nonlinear beams. Theoretical, numerical and experimental analyses. Int. J. Eng. Sci. **145**, 103167 (2019)
46. Pelliciari, M., Sirotti, S., Tarantino, A.M.: A strain energy function for large deformations of compressible elastomers. J. Mech. Phys. Solids **176**, 105308 (2023)
47. Falope, F.O., Lanzoni, L., Tarantino, A.M.: Energetic exhaustiveness for the direct characterization of energy forms of hyperelastic isotropic materials. J. Mech. Phys. Solids **193**, 105885 (2024)
48. Falope, F.O., Lanzoni, L., Tarantino, A.M.: Experiments on the finite torsion of nearly incompressible rubber-like materials: nonlinear effects, analytic modeling and rubber characterization. Int. J. Eng. Sci. **211**, 104254 (2025)